RAA 2021 Vol. **21** No. **12**, 298(10pp) doi: 10.1088/1674-4527/21/12/298

http://www.raa-journal.org *http://iopscience.iop.org/raa*

Research in Astronomy and Astrophysics

Two-telescope-based solar seeing profile measurement simulation

Zi-Yue Wang (王子跃)[1,2,3], De-Qing Ren (任德清)[4] and Raffi Saadetian[4]

[1] National Astronomical Observatories/Nanjing Institute of Astronomical Optics & Technology, Chinese Academy of Sciences, Nanjing 210042, China; *wangziyuebit@163.com*
[2] CAS Key Laboratory of Astronomical Optics & Technology, Nanjing Institute of Astronomical Optics & Technology, Nanjing 210042, China
[3] University of Chinese Academy of Sciences, Beijing 100049, China
[4] Physics & Astronomy Department, California State University Northridge, Northridge, California 91330-8268, USA

Received 2021 June 27; accepted 2021 September 9

Abstract Measurements of the daytime seeing profile of the atmospheric turbulence are crucial for evaluating a solar astronomical site so that research on the profile of the atmospheric turbulence as a function of altitude $C_n^2(h_n)$ becomes more and more critical for performance estimation and optimization of future adaptive optics (AO) including the multi-conjugate adaptive optics (MCAO) systems. Recently, the S-DIMM+ method has been successfully used to measure daytime turbulence profiles above the New Solar Telescope (NST) on Big Bear Lake. However, such techniques are limited by the requirement of using a large solar telescope which is not realistic for a new potential astronomical site. Meanwhile, the A-MASP (advanced multiple-aperture seeing profiler) method is more portable and has been proved that can reliably retrieve the seeing profile up to 16 km with the Dunn Solar Telescope (DST) on the National Solar Observatory (Townson, Kellerer et al.). But the turbulence of the ground layer is calculated by combining A-MASP and S-DIMM+ (Solar Differential Image Motion Monitor+) due to the limitation of the two-individual-telescopes structure. To solve these problems, we introduce the two-telescope seeing profiler (TTSP) which consists of two portable individual telescopes. Numerical simulations have been conducted to evaluate the performance of TTSP. We find our TTSP can effectively retrieve seeing profiles of four turbulence layers with a relative error of less than 4% and is dependable for actual seeing measurement.

Key words: turbulence — atmospheric effects — sun: granulation

1 INTRODUCTION

Researching the vertical altitude distribution of daytime atmospheric turbulence is crucial for nowadays adaptive optics (AO) and multi-conjugate AO (MCAO) (Ren et al. 2018). Many methods have been proposed to measure the profile of daytime optical turbulence. Scharmer & Van Werkhoven proposed a S-DIMM+ (Solar Differential Image Motion Monitor+) technique (Scharmer & van Werkhoven 2010), which was similar to S-DIMM (Solar Differential Image Motion Monitor) (Zhong & Beckers 2001; Beckers et al. 2003; Hill et al. 2006) and was developed from DIMM (Differential Image Motion Monitor) (Sarazin & Roddier 1990; Tokovinin 2002; Wang et al. 2020). The DIMM has become the standard equipment for assessing the atmospheric 'seeing' at astronomical sites (Xu et al. 2020). DIMMs are used for measurements pointing at not only the stellar image but also the Sun (Kawate et al. 2011; Song & Cai et al. 2020; Song et al. 2018). After that, the S-DIMM+ technique was used to measure daytime turbulence profiles above the 1.6-m New Solar Telescope (NST) with 15 sub-apertures of SHWFS (Shack-Hartmann Wavefront Sensor), which yielded a turbulence profile of 4 layers up to 8 km (Kellerer et al. 2012). However, good vertical resolution and high maximum measurement height were obtained with the help of a large-aperture telescope of more than 1 m, which is not realistic for new sites where no large solar facility telescope is available.

Considering the absence of a large solar telescope, Ren proposed a multiple-aperture seeing profiler (MASP) (Ren et al. 2015), which consisted of two portable small telescopes of 400 mm in diameter and can be equivalent to an 1120 mm large telescope. Also, the two 5×5 lenslet arrays of SHWFS can be equivalent to a 14×14 lens let array of SHWFS, which yielded a turbulence profile of 14 layers up to 30 km. Then, to achieve better vertical resolution, Ren introduced an advanced multiple-aperture seeing profiler (A-MASP) (Ren & Zhao 2016), in which two telescopes with a fixed distance and multiple sub-regions on the solar surface with different angular separation served as guide stars that are used to retrieve the atmospheric turbulence seeing profile above the telescope. It yields a vertical resolution of 1000 m and a maximum measurement height of 30 km. However, no matter MASP or A-MASP, the two telescopes, each with its tripod, may have a relative position shift during the seeing profile measurements, which will cause differential orientation error. Due to this reason, the overall Fried parameter can't be obtained directly, as well as the seeing Fried parameter in ground altitude.

In this article, we introduce a new method TTSP (two-telescope seeing profiler) that can obtain good maximum measurement height and vertical resolution without using a large-aperture solar telescope, achieve overall seeing Fried parameter (Chen et al. 2019) to retrieve the strength of the ground-layer turbulence without additional redundant processing steps. In terms of the telescope and the hardware structure, unlike the NST 1.6-meter telescope used by Kellerer et al., we use two small 0.1-meter-diameter telescopes. Unlike the two telescopes installed on their respective tripods in the A-MASP method, we installed two telescopes on the same rigid tripod. In terms of retrieve processing algorithm, The variation of the wavefront distortions with angular direction allows the reconstruction of the distribution of turbulence (Kellerer et al. 2012). In this article, the structure function is related to the variance of differential shifts. It is similar to Kellerer's method, but apparently different from the relationship between the structure function and covariance of differential shifts by A-MASP method.

2 THE PRINCIPLE

To obtain the turbulence seeing profile, the feasibility of using SHWFS instruments (or multiple-apertures seeing profile) has been proved by many authors. And it is even used for solar seeing profile measurements (Kellerer et al. 2012). Our system consists of two telescopes and can be viewed as two aperture Hartmann test devices (Beckers 2001). The two telescopes are jointly fixed on the same rigid tripod, which restricts the two telescopes pointing to the same solar region without relative vibration between them. The rigid tripod is an important piece of equipment that needs to be customized to hold two separate telescopes together to form a binocular equivalent. This can effectively eliminate the relative vibration between the two telescopes caused by wind, telescope vibration or other factors, which ensures that the light paths of the two telescopes are always conjugated at a specific height. Figure 1 shows the layout of

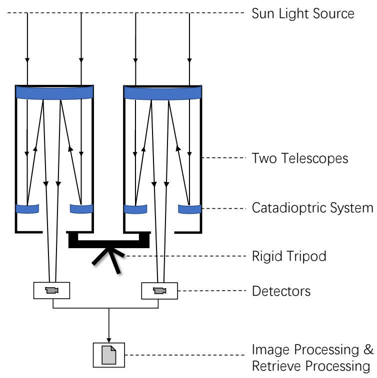

Fig. 1 Layout of TTSP light path and hardware.

TTSP light path and hardware. For the seeing profile measurement, the maximum measurement height and the vertical resolution are two important parameters. The maximum measurement height determines the highest altitude that the SHWFS instrument can measure. The vertical resolution defines the smallest vertical height that the SHWFS instrument can measure. Different from conventional SHWFS observations, in which the angle of two GSs is fixed and it achieves different conjugated heights by choosing sub-apertures combinations with different separation distance, A-MASP, proposed by Ren et al (Ren & Zhao 2016), can achieve a similar effect by choosing GSs combinations with different angular size but with the two aperture sizes and distance are fixed (GS is the abbreviation of guide star in this article) (Sreekanth et al. 2019). As shown in Figure 2, in which each small square represents a solar granule region with a certain size in arcsecond. By combining any two different GSs from the linear array, the different angular sizes between the two GSs are achieved. The conjugate height is given as $H = s/\theta$, where s is the distance between the centers of two telescopes or sub-apertures and is fixed, θ is the angle between the two GSs and is variable. Accordingly, the maximum measurement height is obtained as $H_{\max} = s/\theta_{\min}$, where $\theta_{\min}$ is the minimum angle between two GSs. The vertical resolution is acquired as $H_{\min} = s/\theta_{\max}$, where $\theta_{\max}$ is selected as the maximum angle between two GSs.

Assume that one of the sub-apertures is located at the origin, and the second sub-aperture is located at a distance s from the first sub-aperture. Again, for any GS combination between two GSs, the field angle of the first subfield is assumed to be zero, that of the second subfield is θ, and the third one has an angle of 2θ relative to the first one, and so on. Thus the No.M GS has an angle of $(M-1)\theta$. Furthermore, the variance measurements based on the relative image displacements are either along with longitudinal (x component) or perpendicular (y

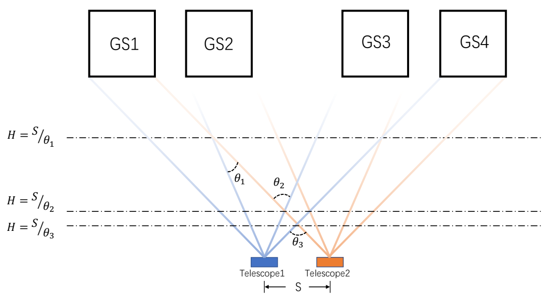

Fig. 2 Schematic diagram.

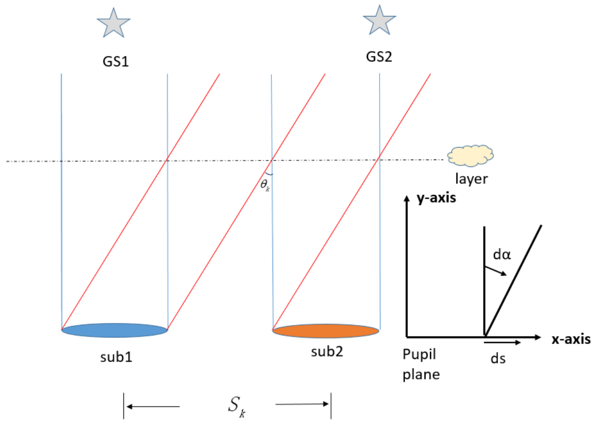

Fig. 3 Layout of the telescopes.

component) to the line connecting the centers of the two sub-apertures. In general, daytime seeing measurements mainly use solar limb or granulation as guide source. For the limb case, the solar differential motions can only be measured in one direction. It uses the longitudinal (or parallel) direction image motion since then any focusing error of the telescope will only result in a systematicly relative displacement of the limb profiles while in the transverse case one would look at two different positions along the limb (Beckers 2001). Unlike the limb case, in this article, we use solar granulation as guide source, which allows us to calculate in both x and y directions. In order to make system calculation convenient and fast, under the premise of science, we only calculate and analyze in x direction. As described earlier, the Fried parameter r_0 retrieve process is similar to Kellerer's method (Kellerer et al. 2012) above the New Solar Telescope (NST) on Big Bear lake. The structure function is related to variance of guide stars' differential shifts, but not the covariance in A-MASP method. For N layers of atmospheric turbulence, which contains ground layer turbulence and $N-1$ turbulences above the ground, the structure functions of the wavefront slopes (along with the x-directions) of each pair of two guide stars are the sum contribution of layers at different altitudes and are determined for the sequence of this pair of stars:

$$D_x(s, d\alpha) = \sum_{n=1}^{N} \left\langle (x_n(0,0) - x_n(s, d\alpha))^2 \right\rangle . \quad (1)$$

$x_n(0,0)$ means the slope of the first guide star located at a height h_n and is measured from the first aperture, while $x_n(s, d\alpha)$ is the slope of the second guide star located at a height h_n and the measurement is achieved from the second aperture. s is the pupil separation along the axis of the sub-apertures (i.e. along the x-axis). $D_x(s)$ represents the variance of differential shifts between two guide stars. $d\alpha$ denotes the angular separation in the vertical plane that contains the x-axis and is numerically equal to θ_k, where $\theta_k = (k-1)\theta$, θ is the angle between two adjacent guide stars and k is the number of the guide stars $k = 1, 2, 3 \cdots N$. See Figure 3.

Sarazin & Roddier (1990) gave approximate expressions for the structure functions of wavefront slopes measured over circular apertures, which was valid for $s > D_{\rm eff}/2$ ($D_{\rm eff}$ is effective diameter and is explained later on). Kellerer et al. modified coefficients for square apertures in terms of 1000 simulated Kolmogorov phase-screens with infinite outer scale and also adjusted the expressions to extend their validity to $s < D_{\rm eff}/2$:

$$\begin{aligned} D_x(s) =& 0.32\lambda^2 r_0^{-5/3} D_{\rm eff}^{-1/3} \\ & \times \left[1 - \frac{0.70}{(s/D_{\rm eff} + 0.70^3)^{1/3}}\right]. \end{aligned} \quad (2)$$

In this article, the structure functions we discuss are the sum contributed by layers at different heights. Then the functions can be eventually calculated as

$$D_x(s) = \sum_{n=1}^{N} c_n F_x(s, \theta_k, h_n). \quad (3)$$

Here, $F_x(s, \theta_k, h_n)$ is the atmospheric function.

$$F_x(s, \theta_k, h_n) = 1 - \frac{0.70}{(s/D_{\rm eff} + 0.70^3)^{1/3}}. \quad (4)$$

The coefficient c_n related to the Fried parameter of each layer is expressed as

$$c_n = 0.32\lambda^2 r_0^{-5/3} D_{\rm eff}(h_n)^{-1/3}. \quad (5)$$

$D_{\rm eff}$ is the effective diameter, and $D_{\rm eff} = d + N_p \alpha_p h$. d is the size of each telescope (0.1 units in meter in this article), N_p equals the number of pixels used for the cross-correlation (10 pixels in this article). α_p denotes the angular size of a pixel (with arcsecond). The local atmospheric refractive index $C_n^2(h_n)$ is related to the local Fried parameter $r_0(h_n)$ as

$$r_0(h_n) = \left[0.423 \left(\frac{2\pi}{\lambda}\right)^2 (\cos\phi)^{-1} C_n^2(h_n) dh\right]^{-3/5}, \quad (6)$$

where λ is the wavelength and ϕ is the zenith angle. The above equation can also be used to calculate the overall Fried parameter r_0 as

$$r_{0(overall)} = \left[0.423\left(\frac{2\pi}{\lambda}\right)^2(\cos\phi)^{-1}\int C_n^2(h_n)\,dh\right]^{-3/5}. \quad (7)$$

Note that when $\theta_k = 0$, it converts to the conventional DIMM. For a linear array of N GSs, there are N pairs of GS combinations whose field angle is zero, namely two telescopes point to the same GS. Then the shift variances of these combinations can be used to solve for the overall Fried parameter that includes the turbulence contributions from the ground to infinite height. Meanwhile, some $(N\times N - N)$ combinations can be used to retrieve the $r_0(h_n)$ in each layer except the ground. This large number of combinations provides enough redundancy to retrieve the seeing Fried parameters, which significantly increases the measurement accuracy (for both the overall Fried parameter measurements and the seeing profile). Because the negative value $r_0(h_n)$ is not physical, the MATLAB lsqnonneg function is used to solve this non-negative least-squares constraints problem. The process of optimization is expressed as follows:

$$\begin{aligned}\min L = &\sum_{s,\theta_k>0}\left(\left[D_x(s,\theta_k) - \sum_{n=1}^{N} c_n F_x(s,\theta_k,h_n)\right]^2\right) \\ &\cdot W^2(\theta_k>0) \\ &+ \sum_{s,\theta_k=0}\left(\left[D_x(s,0) - \sum_{n=1}^{N} c_n F_x(s,0,h_n)\right]^2\right) \\ &\cdot W^2(\theta_k=0), \end{aligned} \quad (8)$$

where $W^2(\theta_k > 0)$ and $W^2(\theta_k = 0)$ are weight functions, and these are used to weigh each guide star combination.

3 SIMULATIONS

3.1 Simulation Software

To test our principle, a series of seeing profiles were generated by a professional optical software YAO, which is coded in Yorick and applies to adaptive optical system simulation (Rigaut & Van Dam 2013). It is widely recognized as a reliable software for simulating point-spread-function imaging under different atmospheres and guide star conditions. YAO can work based on the algorithm required by the system or customizing the wavefront sensor. It avoids the complex process of wavefront reconstruction and provides an interactive interface and good adaptive optical stimulating capability. Figure 4 shows the YAO interface and Figure 5 shows the SH-WFS image sample.

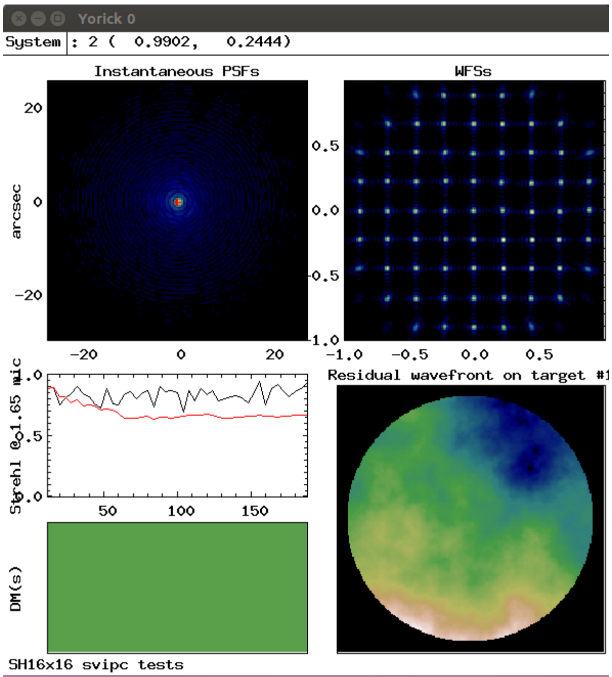

Fig. 4 Software YAO interface.

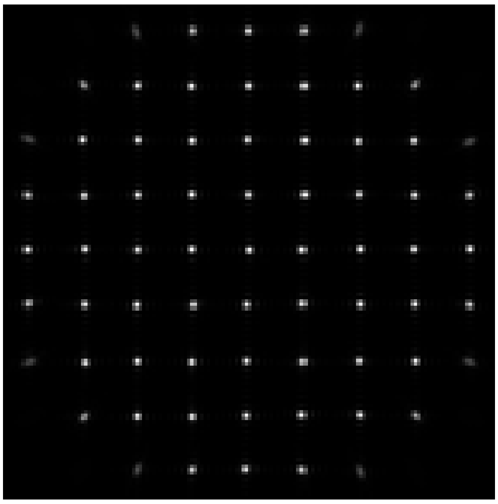

Fig. 5 SH-WFS image sample.

3.2 Situation 1: Retrieve Three Turbulences by Setting one Turbulent Layer at 5 km Height to Verify the Reliability of Software YAO

We set two sub-apertures of diameter 0.1 m with a separation of 0.4 m from a telescope of diameter 1 m. Then we set 4 guide stars, number 1, 2, 3, 4, of which the angular separation of each combination of two guide stars is $\theta(1\&2) = 13.75''$, $\theta(1\&3) = 16.5''$, and $\theta(1\&4) = 20.63''$. The wavefront gradients for different on-sky directions are used to topographically reconstruct atmospheric profiles (Townson et al. 2015) and one pair of two guide stars can only measure one layer, whose height equals to $h = s/\theta_k$. If we already know the height of

Table 1 Angular Separation & Conjugate Altitude

Guide Stars Combination	Angular Separation	Conjugate Altitude (GS1&GSn)
1&2	13.75″	6000 m
1&3	16.5″	5000 m
1&4	20.63″	4000 m

Table 2 YAO Set-up Parameters

YAO Parameter	Setup Values
Telescope Diameter	0.1 m
Apertures Separation	0.4 m
r_0	10 cm
Turbulence Altitude	5 km
Retrieve Layer Heights	4 km, 5 km, 6 km
Guide Star Numbers	4
Pixel Numbers	10
Angular Separations	13.75″, 16.5″, 20.63″
Pixel Size	0.35″
Number of Images	200

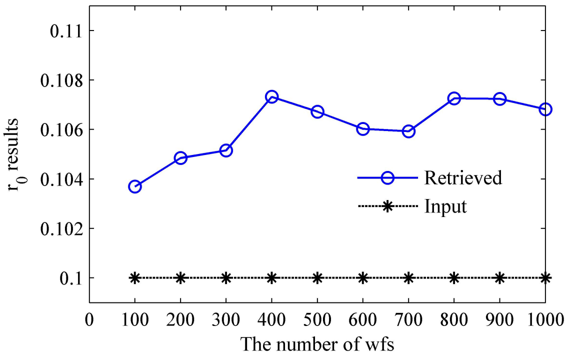

Fig. 6 The results retrieved by 100–1000 images.

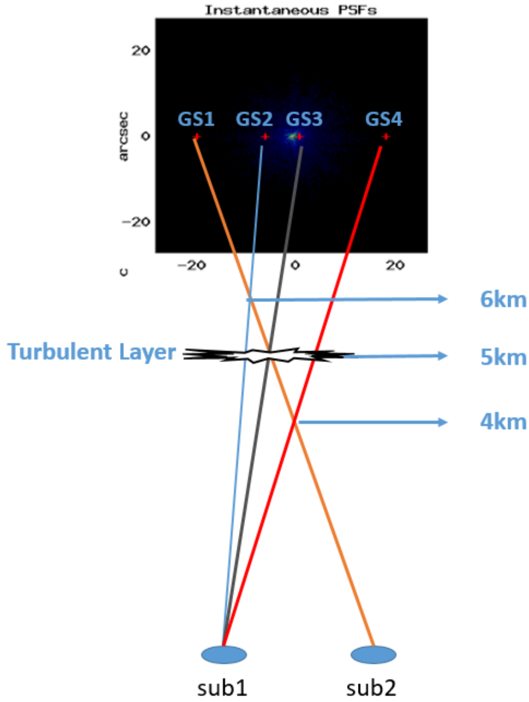

Fig. 7 Diagram of GSs model.

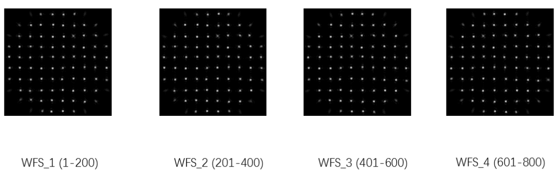

Fig. 8 Diagram of WFSs images.

the turbulent layer is at 5000 m, additional stars are set to retrieve the turbulent layer near 5000 m (respectively 4000 m & 6000 m). Thanks to this, the conjugate altitude obtained by each combination of two guide stars is shown in Table 1. The set-up parameters are shown in Table 2.

In this article, each guide collects 200 images. The reason is that when we compare from 100 to 1000 images, the retrieved results are as shown in Figure 6. We find that the accuracy of the image does not change significantly with the increase in the number of images, but is within the acceptable error range. And when using 200 images, the results are accurate and very satisfactory. See Figure 6.

Figure 7 shows the diagram of GSs mode.

After running the software Yao, we can obtain a total of 800 images at all, in which each guide star contains 200 images separately. Namely, 1–200 images are for GS1, 201–400 for GS2, 401–600 for GS3, and the last 601–800 are for GS4, as shown in Figure 8.

For choosing and extracting the information of GS1 & GS2 combination with angular separation 13.75″, Figure 9 shows the diagram of this process. $x(0,0)$ represents the shift of GS1 obtained by the first aperture and it is indicated by the blue solid circle. The red dotted circle in the left column represents the shift of GS1 captured by the second aperture, whose information is not used. $x(s, d\alpha)$ is extracted from the red solid circle in the right column and represents the shift of GS2 obtained by the second aperture which has an $s = 0.4$ m separation with the first one. Similarly, the information from the blue dotted circle is useless. After repeating the process 200 times, the variance $D_x(dr, d\alpha)$ is obtained via calculating the variance of $[x(0,0) - x(s, d\alpha)]$ or averaging after squaring. Figure 9 shows the diagram of this process.

According to Equation (3), the structure functions are the sum of structure functions contributed by layers at different altitudes. We can rewrite our equations as below:

$$D_x(GS1\&GSk) = \sum_{n=1}^{N} c_n F_x(s, \theta_k, h_n), \tag{9}$$

where $c_n = 0.32\lambda^2 r_0^{-5/3}(h_n) D_{\rm eff}^{-1/3}$.

$$F_x(s, \theta_k, h_n) = 1 - \frac{0.70}{(s/D_{\rm eff} + 0.70^3)^{1/3}}. \quad (10)$$

Equations (9) and (10) are used to fill the matrix M that converts the turbulent energy as a function of altitude, $r_0(h_n)^{-5/3}$, into the structure-function measured at the telescope pupil $D_x(s, d\alpha)$. We assume that the turbulences are concentrated in discrete layers, each with an infinitesimally small thickness, and we can calculate the Fried parameter results at measured altitude above the telescope. In view of this particular situation in this section, the matrix M is shown as below.

$$\begin{bmatrix} D_x(GS1\&GS2) \\ D_x(GS1\&GS3) \\ D_x(GS1\&GS4) \end{bmatrix} = \begin{bmatrix} f_x(s, 4000m) & f_x(s, 5000m) & f_x(s, 6000m) \\ f_x(s, 4000m) & f_x(s, 5000m) & f_x(s, 6000m) \\ f_x(s, 4000m) & f_x(s, 5000m) & f_x(s, 6000m) \end{bmatrix} \begin{bmatrix} r_0^{-5/3}(4000m) \\ r_0^{-5/3}(5000m) \\ r_0^{-5/3}(6000m) \end{bmatrix}, \quad (11)$$

where $f_x(s, h_n) = 0.32\lambda^2 D_{\rm eff}^{-1/3} F_x(s, \theta_k, h_n)$. Then the results are shown in Table 3.

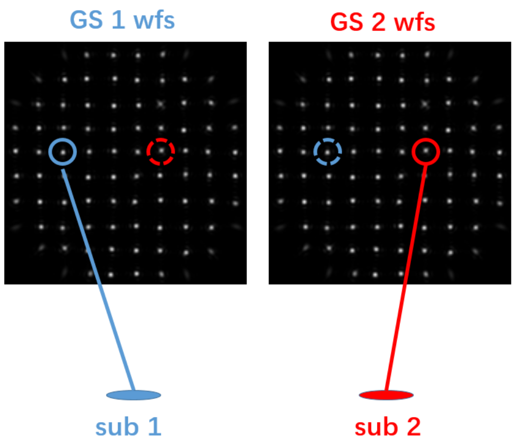

Fig. 9 Diagram of image shifts obtaining by two sub-apertures.

Table 3 Retrieved r_0 Results at Different Heights with Input $r_0 = 10$ cm at 5000 m

$D_s(GS1\&GSk)$	h_n	Retrieved $r_0(h_n)$
$D_s(GS1\&GS4) = 2.35e-12''$	4000 m	19.98 cm
$D_s(GS1\&GS3) = 2.11e-12''$	5000 m	18.99 cm
$D_s(GS1\&GS2) = 2.13e-12''$	6000 m	17.96 cm

The total Fried paramete r_0 we retrieved is via pointing the two telescopes at the same guide star as a DIMM and the result is 9.8 cm, which is 2% different from the input value. The r_0 values for each layer are 19.98 cm at 4000 m, 18.99 cm at 5000 m, and 17.96 cm at 6000 m, and the layer factor of the atmospheric coherence length at different height layers $f(i) = r_0(h_n)^{-5/3}/r_0^{-5/3}$ of each layer is 31.55% at 4000 m, 34.34% at 5000 m, and 37.68% at 6000 m. The total turbulent strength of the layer at 5000 m is divided approximately equally by the adjacent two layers. Due to the infinitesimally small thickness of layers, the strength of adjacent layers is moved to layer at 5000 m iteratively. By comparing set Fried parameter value with retrieved value, r_0 can be accurately retrieved with 2% error, and the software YAO's reliability is verified.

Table 4 YAO Set-up Parameters for Profile 1, 2, 3 & 4

YAO Parameter	Setup Values
Telescope Diameter	0.1 m
Apertures Separation	0.4 m
r_0	10 cm
Retrieve Layer Heights	4 km, 5 km, 6 km
Guide Star Numbers	4
Pixel Numbers	10
Angular Separations	13.75″, 20.63″, 38″
Pixel Size	0.35″
Number of Images	200

4 RESULTS OF THE SEEING PROFILE MEASUREMENTS

In all of the below simulations, we assume that the layer heights are known in advance, aiming to sample the turbulence profile. However, we do not know the turbulence layer number and the height of each layer in advance and in reality. In this case, we can use multiple guide star combinations to increase redundant layers to sample the turbulence profile. We simulate four atmospheric turbulence models, each contains 2, 3, or 4 turbulent layers. The parameters set in YAO are described in Table 4 and the parameters of the four profiles are shown in Table 5. All cases have total $r_0 = 0.1$ m. Profile 1 and 2 represent the case with unknown turbulence layer height. Profile 3 represents the case that layers with relatively regular gradient change, while Profile 4 has relatively uniform change with a much larger contribution for high altitude layers. For each profile, 800 short-exposure images are used to sample the profile.

Table 6 shows the retrieved results of Profile 1 and Profile 2. Though we assume that we do not know the turbulent layer height in advance, multiple guide star combinations provide redundant equations that can be used

Table 5 Input Seeing Profile

	Layer	Strength of Layers	r_0(m)	Altitude(km)
Profile 1	1	0.7	0.124	0
	2	0.3	0.206	3
Profile 2	1	0.5	0.152	0
	2	0.3	0.206	1
	3	0.2	0.263	3
Profile 3	1	0.4	0.173	0
	2	0.3	0.206	1
	3	0.2	0.263	2
	4	0.1	0.398	3
Profile 4	1	0.3	0.206	0
	2	0.3	0.206	1
	3	0.2	0.263	2
	4	0.2	0.263	3

Table 6 Seeing Profile Retrieving Results of Profile 1 and Profile 2

	Input Strength of Layers	Retrieved Strength of Layers	Retrieved r_0(m)	Altitude (km)
Profile 1	0.7	0.74	0.114	0
	0.3	0.26	0.213	3
Profile 2	0.5	0.47	0.154	0
	0.3	0.38	0.176	1
	0.2	0.15	0.306	3

to retrieve the local Fried parameter $r_0(h_n)$ at each layer. For Profile 1, the total Fried parameter r_0 is estimated as 0.095 m, which is 5% different from the input value. The r_0 values for each layer are 0.114 m at 0 km and 0.213 m at 3 km, with relative differences of 8.1% and 3.4%, respectively. For Profile 2, the total Fried parameter r_0 is found as 0.098 m, which is 2% different from the input value. The r_0 values for each layer are 0.154 m at 0 km, 0.176 m at 1 km, and 0.306 m at 3 km. It can be seen that the results indicating the first two lower layers are close to the input values and the result that corresponds to the relative-highest layer of Profile 2 has less accuracy around 15%. The reason is that the results are represented as r_0 units in meter. In the process of retrieving, the percentage of turbulent energy (which is also described in terms of atmospheric refractive index, C_n^2) of each layer is obtained first and the r_0 is the power of –3/5 times of C_n^2, which causes a huge difference between retrieved and input values, even the percentage of turbulent energy of each layer we retrieved is accurate. Still, in Profile 2, the percentages of turbulent energy for each layer are 47.2% at 0 km, 37.8% at 1 km, and 15% at 3 km, with relative differences of 2.8%, 8.7%, and 5% respectively, which is in an acceptable range (for example, the induced retrieved C_n^2 error must be less than 10%.).

Figure 10 shows the retrieved $C_n^2(h_n)$ results of Profile 3 and Profile 4. To the left of Figure 10 is the proportion of the strength of the layers that are retrieved. The blue solid line indicates the retrieved results, while the black bar shows the input results. From the left column, we can see four layers located at 0 km, 1 km, 2 km, and 3 km for both Profile 3 and Profile 4. All four layers in each profile are resolved. To the right column of Figure 10, the cumulative $C_n^2(h_n)$ from each layer is plotted. The blue dashed line indicates the retrieved results, while the black solid line shows the input results. For Profile 3, the total Fried parameter r_0 we retrieved is 0.094 m, which is 6% different from the input value of 0.1 m. The fractional atmospheric refraction index $C_n^2(h_n)$ values for each layer are 39.22%, 28.75%, 21.86%, and 10.17% with 0.8%, 1.3%, 1.9%, and 0.2% relative difference. For Profile 4, the total Fried parameter we found is 0.0938 m, which has a 6.2% error. The fractional atmospheric refraction index $C_n^2(h_n)$ values for each layer are 31.42%, 26.05%, 22.53%, and 20.01% with relative difference of 1.4%, 4%, 2.5%, and 0.01%, respectively. The results show that our new approach has excellent sensitivity and good capability to retrieve multiple turbulence layers.

Table 7 Seeing Profile Retrieving Results of Profile 5

	Input Strength of Layers	Retrieved Strength of Layers	Relative Difference	Altitude (km)
Profile 5	0.4	0.43	3%	0
	0.3	0.26	4%	3
	0.2	0.17	3%	8
	0.1	0.14	4%	12

Continue to research and further verify our approach, we simulate one more atmospheric turbulence model: Profile 5 with four discrete layers at 0 km, 3 km, 8 km, and 12 km. The measurement obtained at BBSO (Big Bear Solar Observatory) indicated that the day-time turbulence profile is distributed on four layers and have three origins: (1). a ground layer (from the ground to 500 m above the ground) (Liu et al. 2010) that comprises 55%–65% of the turbulence; (2). a boundary layer between 1–7 km contains 30%–40% of the turbulent energy; (3). the remaining around 5% is distributed in the tropopause, which is above 12 km in summer and between 8–12 km in winter. The setup parameters and retrieve results of Profile 5 are shown in Table 7.

For Profile 5, the total Fried parameter r_0 we found is 0.0945 m, which has 5.5% error. The fractional atmospheric refraction index $C_n^2(h_n)$ values for each layer are 42.50%, 26.38%, 17.22%, and 13.89% with 3%, 4%, 3%, and 4% relative difference.

Profile 5 is designed to test whether the TTSP method can effectively and accurately retrieve the values of turbulence at each layer. Although we referred to Kellerer's profile values on Big Bear Lake, they are still different after all. In order to simulate the atmospheric turbulence profile of the NST on Big Bear Lake more realistically, we used the Hufnagel-Valley-Boundary (HVB) model (Hill et al. 2003) to simulate 0–7000 m turbulence profile. Based on

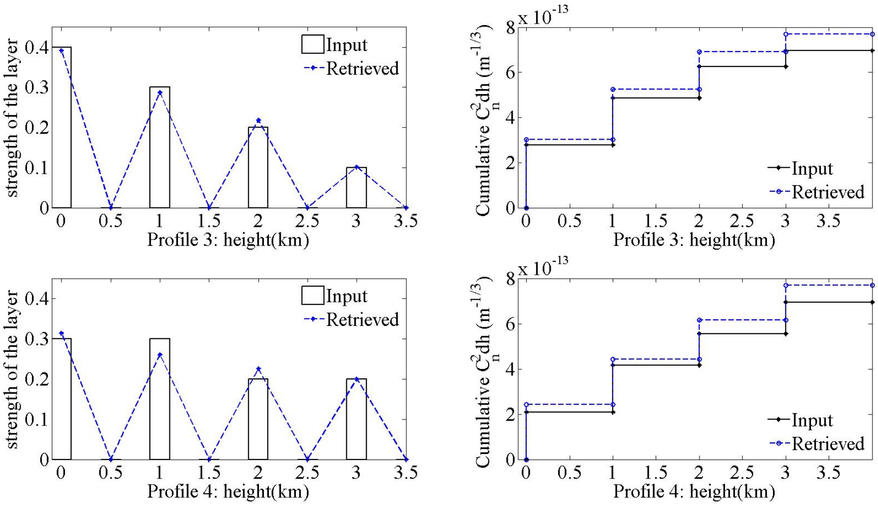

Fig. 10 $C_n^2(h_n)$ results of Profile 3 and Profile 4.

the Hufnagel-Valley model commonly used in the night-time atmosphere, the HVB model considers the effects of the day-time atmospheric boundary layer, and can reflect the distribution characteristics of the atmospheric turbulence during the day. In HVB model, a daytime turbulence profile can be represented as:

$$C_n^2(h) = C_{nHV}^2(h) + A_B \exp(-h/h_0). \tag{12}$$

The first part to the right of Equation (12) is the Hufnagel-Valley model, which is mainly used to calculate the night turbulence profile, which can be represented as:

$$C_{nHV}^2(h) = A_{HV}\left[2.2\times10^{-23}\left(\frac{h+z}{1000}\right)^{10} \times \exp\left(-\frac{h+z}{1000}\right) + 10^{-16}\exp\left(-\frac{h+z}{1500}\right)\right]. \tag{13}$$

The HV profile is a good approximation to $C_n^2(h)$ for night time conditions. For a better model of a daytime $C_n^2(h)$, the second part to the right of Equation (12) is for adding additional turbulence near the ground. Thereinto, A_{HV} and A_B are chosen amplitudes, z is the elevation of the site in meters, and h_0 is the height of boundary layer. In the process of setting input values, according to Kellerer's result, $r_0 = 0.091$ m at 550 nm wavelength in summer. It is equivalent to $r_0 = (500/550)^{6/5}(0.091\mathrm{m}) = 0.081$ m at 500 nm wavelength. We set amplitude $A_{HV} = 0.25$, $A_B = 0.95 \times 10^{-15}$, the elevation of the site is $z = 2000$ m, and the boundary height $h_0 = 1000$ m. In the process of simulating, both telescopes have a 0.1m-aperture in diameter, and the separation between the telescopes is set 0.3 m. Figure 11 shows the HVB simulated turbulence profile curve.

For $0 - 7000$ m, the turbulence profile we simulated fits very closely to the result of the input parameters

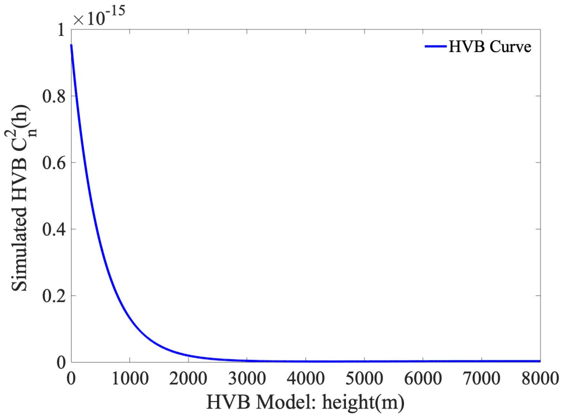

Fig. 11 Turbulence profile $C_n^2(h)$ results simulated by HVB model.

gotten by Kellerer et al. In this height range, the total strength of the turbulence profile simulated by HVB is only 0.19×10^{-13} difference from the input value. Not only that, but in $0 - 1000$ m, $1000 - 2000$ m, and $2000 - 7000$ m intervals, the cumulative atmospheric refractive index $C_n^2(h)$ approximately equals to the input value. Table 8 shows the cumulative $C_n^2(h)$ values of HVB intput and output.

5 CALCULATING TURBULENCE WITH TWO INDIVIDUAL TELESCOPES

Based on our approach, our instrument can not only use a pupil mask to make two sub-apertures as S-DIMM+ did, or install two telescopes on a rigid tripod as an integrated unit like A-MASP did. However, our instrument with two individual telescopes fixing on the same tripod has a significant difference from the real A-MASP system that as well uses two separate telescopes. For both systems, the two telescopes may have a relative position shift in

Table 8 The Cumulative $C_n^2(h)$ Values of HVB Intput and Output

Height Range	Input cumulative $C_n^2(h)$	HVB Output cumulative $C_n^2(h)$
0–1000 m	6.23×10^{-13} m$^{1/3}$	6.05×10^{-13} m$^{1/3}$
1000–2000 m	2.05×10^{-13} m$^{1/3}$	2.23×10^{-13} m$^{1/3}$
2000–7000 m	1.55×10^{-13} m$^{1/3}$	1.36×10^{-13} m$^{1/3}$
0–7000 m	9.84×10^{-13} m$^{1/3}$	9.65×10^{-13} m$^{1/3}$

each short exposure due to the guiding error or vibration. In Ren et al. (2015), Ren proposed a technique, which can effectively remove the relative position shift between the two telescopes. Due to the structure functions in Ren et al. (2015) are related to the covariance of guide star displacement, the first measurement δx_1 is the added contributions of each layer located at a height h_n

$$\delta x_1(s,0) = \sum_{n=1}^{N}(x_n(s) - x_n(0)), \tag{14}$$

where $x_n(0)$ means the slope of the first guide star and the measurement is achieved from the first telescope, while $x_n(s)$ means the slope of the first guide star and the measurement is achieved from the second telescope. For the second measurement δx_2, which is a function of the differential shift of the second subfield.

$$\delta x_2(s,\theta_k) = \sum_{n=1}^{N}\left(x_n(s+\theta_k h_n) - x_n(\theta_k h_n)\right), \tag{15}$$

where $\theta_k = (k-1)\theta$. The modified equations for the two-individual-telescopes case are shown as:

$$\langle \delta x_1 \delta x_2 \rangle = \sum_{n=1}^{N} c_n F_x(s,\theta_k,h_n) + \Delta_x. \tag{16}$$

Where

$$\begin{aligned}\Delta_x = &< \delta x_1^2 > /2 + < \delta x_2^2 > /2 \\ &- \sum_{n=1}^{N} c_n I(s/D_{\rm eff}, 0)\end{aligned} \tag{17}$$

is the displacement between the two telescopes in each short exposure and is used to remove the relative position shift on the x and y-direction, respectively.

If $\theta = 0$, which means two telescopes point at the same target and A-MASP obtains:

$$\begin{aligned}< \delta x_1^2 > &= \sum_{n=1}^{N} c_n F_x(s,0,h_n) + \Delta_x \\ &= \sum_{n=1}^{N} c_n I(s/D_{\rm eff},0) + < \delta x_1^2 > /2 \\ &\quad + < \delta x_1^2 > /2 - \sum_{n=1}^{N} c_n I(s/D_{\rm eff},0) \\ &= < \delta x_1^2 > .\end{aligned} \tag{18}$$

Equation (18) donates no information about structure functions. When A-MASP with two individual telescopes pointing at the same target is not equivalent to conventional DIMM, the total r_0 cannot be retrieved. Thereby, the strength of the ground layer at altitude $h = 0$ cannot be measured by A-MASP directly, either. As a result, A-MASP has to add an extra step that obtains the total Fried parameter by method S-DIMM, and then the turbulence of the ground layer can be calculated by combining the results of those two methods.

On the contrary, the structure functions of wavefront slopes in our TTSP are determined by the variance of relative position shift. Also use the above-modified Equations (9) & (10), the left side of the equation is the variance of one guide star displacement measured through two individual telescopes, which is the same with the left term of Equation (18) and the right term of Equation (9) provides the information of structure functions to retrieve the seeing parameters. In this case, TTSP, as one binocular instrument, can effectively eliminate guide error caused by telescope shaking. So, the total r_0 can be retrieved as well as the turbulence of the ground layer. It leads to a new guess that even two-separate-telescopes structure does not affect our approach. The premise is ignoring extreme cases, such as random jitter between two telescopes.

6 ERROR ANALYSIS AND DISCUSSION

The relative difference in our simulation is attributed to three main reasons: (1). The contrast of the structure functions decreases with altitude. Because the slopes are computed through a cross-correlation over a field of a finite size that is averaged over larger surfaces with increasing altitude. Due to this impact, results in some layers are with a relatively large difference and in some other layers are with negative values, which is not physical. So, our optimization method is utilized. (2). Results in Profile 1–5 are all obtained by relatively coarse optimization. Since the results have been good proof that our method can clearly distinguish the four-layer turbulence, to meet the needs of the seeing profile measurement, so there is no deliberate pursuit of higher optimization accuracy. (3). Increasing the number of guide star combinations can increase the density of turbulence layers and improves measurement accuracy. Because when the layer number increases, more equations will be needed to ensure enough redundancy for accurate retrieving.

Furthermore, the guide star pairs with large angular separation will provide better vertical resolution at a lower height. which has strong turbulence and is more essential for the AO system. For example, in Profile 3, the vertical resolution is acquired by $\delta h = s/\theta = 0.2\text{m}/38'' = 1000$ m. If guide star combination with a larger separation of $76''$ is used, the vertical resolution is much better as

500 m. The same effect can be obtained by changing the separation distance between the two telescopes.

7 CONCLUSION

We propose a Two-Telescope-Based Solar Seeing Profiler (TTSP) for precision solar seeing profile measurements. The new method consists of two small telescopes, each with a 10 cm aperture. TTSP uses a linear array of guide stars to retrieve the seeing profile. Since any number of guide star combinations can be used, via changing the proper separation of guide star pairs or distance between two apertures, our approach can have good vertical resolution and satisfactory maximum sample height. In our paper, we demonstrated the cases that seeing profiles with four layers can be effectively retrieved with a precision better than 4%. For all situations, the r_0 values are in line with science, that is, the larger the height, the lower the fraction of atmospheric turbulence, and the larger the r_0 value. As the altitude increases, the r_0 values are dissipated. Our approach can omit the additional step, for example, A-MASP uses two small telescopes, each with its own tripod, to measure daytime turbulence profiles. In order to eliminate the pointing error produced by shaking in the observation of the two telescopes, additional corrections were introduced in the turbulence profile measurement retrieve algorithm. The corrections cause the atmospheric turbulence intensity to be unmeasurable at the height of the turbulence layer $h = 0$. To make up for this deficiency, MASS or other methods have to be extra added. Unlike A-MASP, The two telescopes in TTSP are jointly fixed on the same rigid tripod, which restricts the two telescopes pointing to the same solar region and keeps the light paths conjugated without either relative vibration or guide errors. Also TTSP avoids combining with MASS to get ground Fried parameter. It can easily obtain the total Fried parameter when calculating the differential shifts information from only one guide star through two telescopes so that to retrieve every refractive index $C_n^2(h_n)$ at each height. And TTSP does not need to use Shack-Hartmann wavefront sensor, which can also effectively eliminate the SHWFS with relatively low resolution, limited dynamic range, and difficult precision calibration. It makes our instrument more convenient to carry. Considering that no large facility telescope is available at the new site, or even with existing large telescopes, it is difficult to apply for a large amount of observation time, our method is portable and effective to measure the seeing profile for future solar MCAO system.

Acknowledgements The author Ziyue Wang acknowledges the partially support by National Nature Science Foundation of China (Grant Nos. U2031210 and 11873068), Special Fund for Research on National Major Research Instruments (Grant No. 11827804).

References

Beckers, J. M. 2001, Experimental Astronomy, 12, 1

Beckers, J. M., Liu, Z., & Jin, Z. 2003, in Innovative Telescopes and Instrumentation for Solar Astrophysics, SPIE Conference Series, 4853, 273

Chen, L. H., Liu, Z., & Chen, D. 2019, RAA (Research in Astronomy and Astrophysics), 19, 149

Hill, F., Radick, R., & Collados, M. 2003, Deriving $C_n^2(h)$ from a Scintillometer Array, https://atst.nso.edu/sites/atst.nso.edu/files/docs/RPT-0014-A.pdf

Hill, F., Beckers, J., Brandt, P., et al. 2006, in SPIE Conference Series, 6267, 62671T

Kawate, T., Hanaoka, Y., et al. 2011, MNRAS, 416, 2154

Kellerer, A., Gorceix, N., Marino, J., et al. 2012, A&A, 542, A2

Liu, L. Y., Yao, Y. Q., Wang, Y. P., et al. 2010, RAA (Research in Astronomy and Astrophysics), 10, 61

Ren, D. Q., Zhang, X., & Liu, S. Z. 2018, RAA (Research in Astronomy and Astrophysics), 18, 086

Ren, D. Q., & Zhao, G. 2016, PASP, 2016, 128, 105002

Ren, D. Q., Zhao, G., et al. 2015, PASP, 127, 870

Rigaut, F., & Van Dam, M. 2013, Proceedings of the Third AO4ELT Conference, eds. S. Esposito, & L. Fini, 18

Sarazin, M., & Roddier, F. 1990, A&A, 227, 294

Scharmer, G., B., & van Werkhoven, T. I. M. 2010, A&A, 513, A25

Song, T., Cai, Z., Liu, Y., et al. 2020, MNRAS, 499, 1909

Song, T. F., Wen, Y. M., Liu, Y., et al. 2018, Sol. Phys., 293, 37

Sreekanth, R. V., Banyal, R. K., Sridharan, R., et al. 2019, RAA (Research in Astronomy and Astrophysics), 19, 125

Tokovinin, A. 2002, PASP, 114, 1156

Townson, M. J., Kellerer, A., Osborn, J., et al. 2015, Journal of Physics: Conference Series, 595, 012035

Wang, J. F., Tian, J. F., Zeng, X. Q., et al. 2020, RAA (Research in Astronomy and Astrophysics), 20, 55

Xu, J., Ali, E., et al. 2020, RAA (Research in Astronomy and Astrophysics), 20, 86

Zhong, L., & Beckers, J. M. 2001, Sol. Phys., 198, 197